IEEE Access
Multidisciplinary ⋮ Rapid Review ⋮ Open Access Journal

Received June 18, 2020, accepted July 7, 2020, date of publication July 15, 2020, date of current version July 24, 2020.

Digital Object Identifier 10.1109/ACCESS.2020.3009294

Monocular Vision-Based Earth's Graviation Method Used for Low-Frequency Vibration Calibration

MING YANG[1], HAIJIANG ZHU[1], CHENGUANG CAI[2], YING WANG[3,4], ZHIHUA LIU[2], AND SHENGYANG ZHOU[1]

[1]College of Information Science and Technology, Beijing University of Chemical Technology, Beijing 100029, China
[2]National Institute of Metrology, Beijing 100029, China
[3]Institute of Microelectronics, Chinese Academy of Sciences, Beijing 100029, China
[4]School of Microelectronics, University of Chinese Academy of Sciences, Beijing 100049, China

Corresponding authors: Chenguang Cai (caichenguang@nim.ac.cn) and Ying Wang (wangying@mail.buct.edu.cn)

This work was supported in part by the National Key Research and Development Program of China under Grant 2017YFF0205003, in part by the Quality and Technical Supervision Ability Promotion Project under Grant ANL1820, and in part by the National Natural Science Foundation of China under Grant 51605461.

ABSTRACT At present, the sensitivity phase of low-frequency accelerometer is commonly calibrated by time synchronization (TS), which needs to strictly align its input excitation acceleration signal and output signal in the time domain. However, TS is very difficult to be implemented and has severely restricted the improvement of the measurement accuracy. A novel calibration method that combines the monocular vision method and time-spatial synchronization technique is investigated to achieve the high-accuracy sensitivity phase calibration. The sensitivity phase is accurately calibrated by determining the aligned spatial position between the excitation acceleration signal and the output signal with the monocular vision method. The sensitivity magnitude can also be simultaneously calibrated. Experimental results show that the calibrated sensitivity phase and magnitude by the investigated method agree well with those by the laser interferometry in the range from 0.3 Hz to 2 Hz. The calibration accuracy of the investigated method is especially superior to that of the laser interferometry in the range from 0.01 Hz to 0.3 Hz.

INDEX TERMS Low-frequency accelerometer, sensitivity phase and magnitude, monocular vision, time-spatial synchronization (TSS), laser interferometry.

I. INTRODUCTION

The low-frequency accelerometer is increasingly being applied to monitor the vibration in the fields such as bridge and building structure safety testing, earthquake warning, wind power safety, etc [1]–[4]. The accurate sensitivity phase and magnitude of the accelerometer is the prerequisite to ensure the vibration monitoring accuracy. To realize high-accuracy low-frequency vibration measurement, a better calibration method should be developed to accurately determine the sensitivity phase and magnitude [5].

The vibration calibration is commonly accomplished by the comparison method (CM) [6] and the laser interferometry (LI) recommended by ISO 16063-11 and 16063-41 [7], [8]. The CM is not suitable for high-accuracy sensitivity magnitude calibration, because its calibration accuracy depends on the uncertainty of the reference accelerometer which is usually calibrated by LI, and it cannot calibrate the sensitivity phase. The sensitivity magnitude uncertainty nears to 0.1% by LI with some improvements reported in [9]–[11], or is even lower at specified laboratory conditions. However, the sensitivity phase calibration accuracy is only 0.5° which is insufficient for the high-accuracy calibration when the frequency is $>$ 0.3 Hz. Furthermore, the sensitivity phase and magnitude calibration accuracy by LI are significantly decreased because the excitation acceleration provided by the shaker with a limited stroke leads to the low SNR output signal of the accelerometer when the frequency is $<$ 0.3 Hz [12], [13]. The Earth's gravitation (EG) method described in [14] uses a rotator to provide the sinusoidal excitation acceleration at a constant high-amplitude to the accelerometer, which avoids the small excitation acceleration

The associate editor coordinating the review of this manuscript and approving it for publication was Akansha Singh.

of LI when the frequency is < 0.3 Hz. However, its sensitivity phase calibration accuracy is also around 0.5° because there is an extra uncertainty caused by the difference between the reference direction and the real direction of the Earth's gravitational field. Considering that the excitation acceleration of the EG method depends on the rotation angle of the rotator, the monocular vision (MV) method is adopted to measure the rotation angle.

Currently, the MV method has been applied to measure the angle because of its briefness, efficiency, and flexibility [15]–[18], whose measurement accuracy even reaches to several arc seconds as described in [19], [20]. We propose a monocular vision-based Earth's gravitation (MVEG) method to calibrate the sensitivity phase and magnitude of the low-frequency accelerometer. The MV method is used to orient the Earth's gravitational field and measure the rotator rotation angle in order to determine the excitation acceleration applied to the accelerometer. The excitation acceleration signal of the accelerometer and its output signal should be synchronously collected to calibrate the sensitivity phase by the TS. However, the synchronous collection is actually difficult, which leads to an extra uncertainty. We accomplish the sensitivity phase calibration based on the time-spatial synchronization (TSS). The sensitivity phase is calculated by the phase of the excitation acceleration signal and that of the output signal at the aligned zero spatial position of the rotator. Because the zero-encoder installed on the rotator outputs the pulse signal when the rotator passes through the zero position, the phase of the output signal is obtained by detecting the time of the pulse signal. Its corresponding spatial position is aligned with the spatial position of the excitation acceleration signal at the zero position which is measured by the MV method.

The rest of this paper is structured as follows. In Section II, the MVEG low-frequency accelerometer calibration system is described. The sensitivity phase and magnitude calibration method based on the monocular vision method and the time-spatial synchronization technique is described in detail in Section III. Section IV provides experimental results and the discussion, and the conclusion is given in Section V.

II. SENSITIVITY PHASE AND MAGNITUDE CALIBRATION SYSTEM OF LOW-FREQUENCY ACCELEROMETER

Figure 1 shows a schematic of the MVEG low-frequency accelerometer calibration system. The rotator provides the sinusoidal excitation acceleration at a constant amplitude and specified frequency to the accelerometer under test (AUT). The zero-encoder installed on the rotator outputs a pulse when the rotary surface of the rotator passes through its zero position. The plumb is putted into a sink filled with oil to reduce the air disturbances to the plumb line. The direction of the plumb line is the same as that of the Earth's gravitational field. The AUT and the mark are firmly mounted on the rotary surface. The long edges of the rectangle in the mark are parallel to the sensitive axis direction of the AUT, which have the consistent rotation angle with the AUT. The spatial position

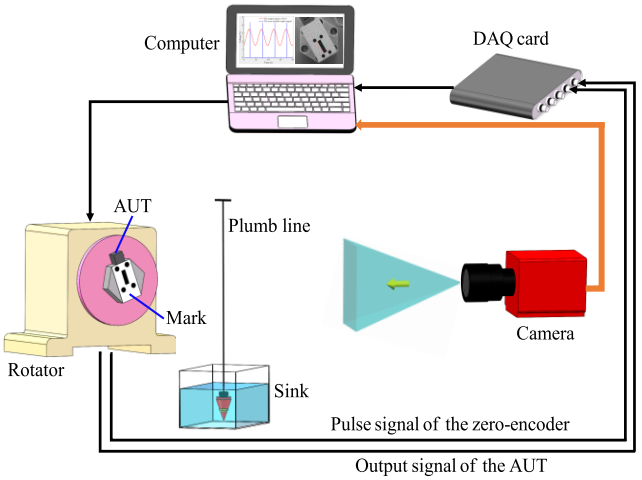

FIGURE 1. Schematic of the MVEG low-frequency accelerometer calibration system.

of the excitation acceleration signal at the zero position for calibrating the sensitivity phase is got by measuring the angle between the long edge at different rotation positions and the plumb line by the MV method. The camera and the DAQ card are used to collect the images of the plumb line and the mark, output signal of the AUT and pulse signal of the zero-encoder, respectively.

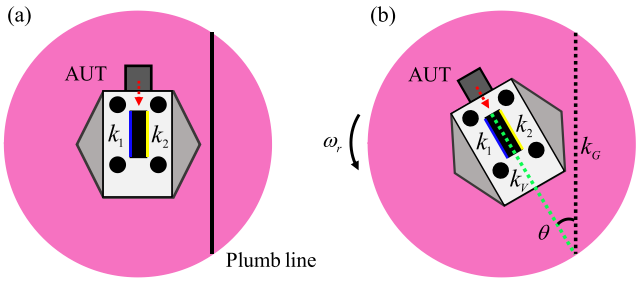

FIGURE 2. Sketch of the collected images. (a) The plumb line at the stationary position, and (b) the mark at the rotation position.

As shown in Fig. 2, the rectangle is embraced in the ROI composed of the centers of the four circles in the mark. The sensitive axis direction of the AUT (the red dotted line) is parallel to the long edges of the rectangle with the slopes k_1 and k_2. k_V (the green dotted line shown in Fig. 2(b)) is the average value of k_1 and k_2, which denotes the direction of the sensitive axis. The rotary angular frequency of the rotator is ω_r. The plumb line direction k_G is the direction of the Earth's gravitational field. The rotation angle from the sensitive axis to the plumb line is θ, which can be calculated by k_V and k_G. The value of θ is 0° when the sensitive axis direction is parallel to the direction of the Earth's gravitational field. The excitation acceleration of the AUT is $g_{loc} \cos(\theta)$ when the rotation angle is θ [14], where g_{loc} is the local gravitational acceleration.

III. SENSITIVITY PHASE AND MAGNITUDE CALIBRATION METHOD

The θ is measured using the collected images of the mark and the plumb line by the MV method, then the excitation

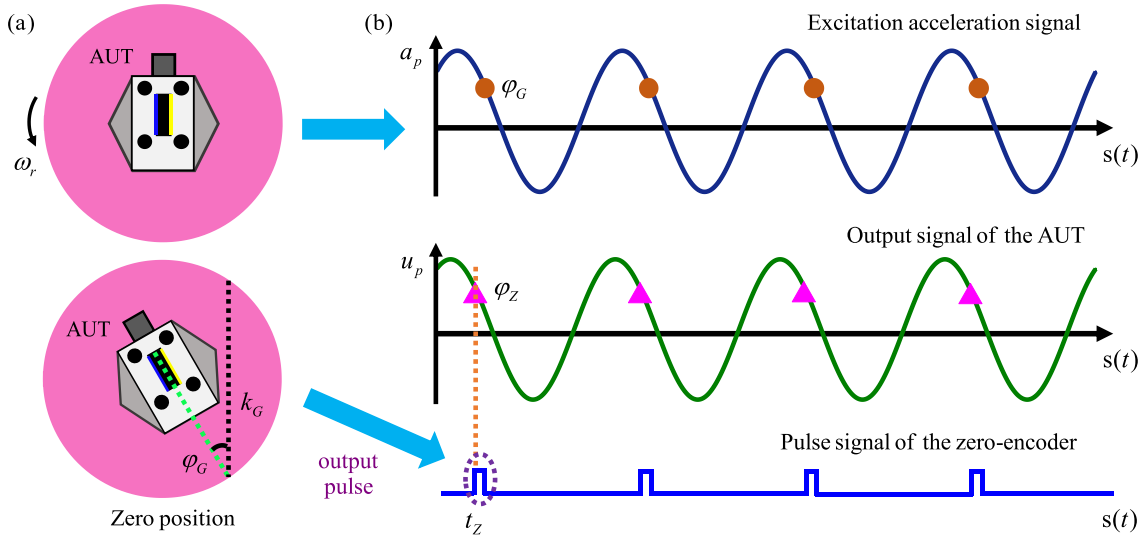

FIGURE 3. The image of the mark at the rotation position and zero position, respectively, and (b) the excitation acceleration signal of the AUT measured by the MV method, output signal of the AUT, and pulse signal of the zero-encoder in the spatial domain.

acceleration of the AUT can be calculated. The sensitivity phase of the AUT is the difference of the phase at the aligned spatial position of the excitation acceleration signal and the phase of its output signal at the zero position. As shown in Fig. 3, the excitation acceleration signal (the periods are four) is got by measuring the θ at different rotation positions, the pulse signal and the output signal are synchronously collected. The rotary surface passes through its zero position once at each period. Take the first period as example, when the rotary surface is at the zero position, the phase of the excitation acceleration signal is φ_G. Meanwhile, the output pulse time of the zero-encoder is t_Z, and the corresponding phase of the output signal at t_Z is φ_Z.

Because φ_G and φ_Z are the phases of the input excitation acceleration signal and output signal of the AUT corresponds to the aligned spatial position, the sensitivity phase φ_p of the AUT is calculated by:

$$\varphi_p = \varphi_Z - \varphi_G, \tag{1}$$

calibrated by the TSS, φ_p avoids the uncertainty caused by the asynchronous acquisition between the mark images and the output signal of the AUT. The collected output signal $u\,(t_i)$ at sampling time t_i is fitted by the sine approximation method (SAM) [24]:

$$u\,(t_i) = A_u \cos\,(\omega_r t_i) - B_u \sin\,(\omega_r t_i) + C_u t_i + D_u, \tag{2}$$

where, $i = 1, 2, \ldots, H$, and H is the sampling number. A_u, B_u, C_u, and D_u are calculated by solving the H equations with H different time t_i and $u\,(t_i)$ as Eq. (2). The fitted amplitude is $\sqrt{A_u^2 + B_u^2}$, and initial phase φ_s is $\arctan(B_u/A_u)$. Then the φ_Z of the output signal at t_Z is calculated by

$$\varphi_Z = \arcsin\,(\varphi_s + \omega_r t_Z) \cdot 180/\pi. \tag{3}$$

The excitation acceleration is related to the rotation angle θ and the g_{loc}. θ is measured by the direction of the Earth's gravitational field and that of sensitive axis of the AUT, which depended on the extraction accuracy of the plumb line and the long edges. The skeleton extraction method is adopted to extract the center points of the plumb line in the image (as shown in Fig. 2(a)). These extracted center points are fitted by the least squares fitting method to obtain the slope k_G of the plumb line.

The ROI is detected by matching the circles in the image to avoid the disturbance of other similar edges before extract-ing the long edges. A series of circle templates $\{T_j\}$ with different sizes are selected to match the circles, where j is $1, 2, \ldots, S$, and S is the number of the templates. These templates ensured that the circles in the image captured at different rotation positions and distances can also be matched correctly [21]. Only the region that has the maximum correlation coefficient $R_j(x, y)$ with T_j is the matched circle. The $R_j\,(x, y)$ is calculated by the formula:

$$R_j\,(x, y) = \frac{\sum_{u=1}^{M}\sum_{v=1}^{N} P\,(x+u, y+v)\,Q\,(u, v)}{\sqrt{\sum_{u=1}^{M}\sum_{v=1}^{N}[P\,(x+u, y+v)]^2 \sum_{u=1}^{M}\sum_{v=1}^{N}[Q\,(u, v)]^2}}, \tag{4}$$

where M and N are the row and column of the jth template, $P\,(x+u, y+v) = F\,(x+u, y+v) - \bar{F}$, $F(x, y)$ is the mark image, and $Q\,(u, v) = T_j\,(u, v) - \bar{T}_j$. $\bar{F}$ and $\bar{T}_j$ are the average grayscale values of $F(x, y)$ and the jth template, respectively.

The Zernike moment sub-pixel edge detection method with the three-grayscale edge model [22], [23] is adopted to extract the long edges. The sub-pixel coordinates of the edge point are depicted as parameters d_1, d_2, and ϕ. The Zernike moments Z_{nm} of $F(x, y)$ are calculated by the convolution of $F(x, y)$ and Zernike moment template. In which, n is a non-negative integer, and m is an integer subjecting to the constraint that $n - |m|$ is a non-negative even number. The moments of Z_{nm} rotated ϕ are defined as:

$$Z'_{nm} = Z_{nm} e^{-im\phi}. \tag{5}$$

The d_1, d_2, ϕ are calculated by the following formulas:

$$d_1 = \sqrt{\frac{5Z'_{40} + 3Z'_{20}}{8Z'_{20}}}, \quad d_2 = \sqrt{\frac{5Z'_{31} + Z'_{11}}{6Z_{11}}}, \tag{6}$$

$$\phi = \tan^{-1}\left(\frac{\mathrm{Im}\,[Z_{31}]}{\mathrm{Re}\,[Z_{31}]}\right), \tag{7}$$

where Im $[Z_{31}]$ and Re $[Z_{31}]$ are the imaginary and real parts of Z_{31}, respectively. The sub-pixel coordinate of the long edge point is calculated by:

$$\begin{bmatrix} x_{sub} \\ y_{sub} \end{bmatrix} = \begin{bmatrix} x_0 \\ y_0 \end{bmatrix} + \frac{K\,(d_1 + d_2)}{4} \begin{bmatrix} \cos\phi \\ \sin\phi \end{bmatrix}, \tag{8}$$

where $(x_0,\ y_0)$ is the pixel coordinate of the edge point extracted by the canny method, and K is the size of the Zernike moment template. The least squares fitting method is used to fit the extracted sub-pixel edge points. The average value k_V is calculated by the slopes k_1 and k_2 of these two fitted long edges. θ is calculated by k_G and k_V, and the excitation acceleration of the AUT is got by $g_{loc}\cos(\theta)$.

Similarly, the SAM shown as Eq. (2) is used to fit the excitation acceleration by the MV method, then the A_V, B_V, C_V, and D_V are obtained. The φ_G of the excitation acceleration at the zero position is calculated by:

$$\varphi_G = \arcsin\left[\frac{a\,(t_Z) + D_V}{g_{loc}}\right] \times 180/\pi. \tag{9}$$

By formulas (3) and (9), the phase φ_Z of the output signal and the phase φ_G of the excitation acceleration signal at the aligned spatial position are calculated. The sensitivity phase φ_p is calculated by formula (1) at each aligned position in the entire sampling period (For example, the aligned positions in Fig. 3(b) are four). The average value of φ_p is taken as the sensitivity phase to reduce the uncertainty.

According to ISO 16063-11, the sensitivity magnitude of the AUT is the ratio of fitted amplitude of its output signal to the excitation acceleration amplitude g_{loc}. The sensitivity magnitude can be easily obtained by measuring the amplitude of output signal of the AUT.

IV. EXPERIMENTAL RESULTS AND DISCUSSION

Figure 4 is the calibration setup for low-frequency accelerometer. A rotator with a range from DC to 2 Hz provided the sinusoidal excitation acceleration to the AUT (MSV 3100A), which was firmly mounted on the rotatory surface. A high-contrast mark, comprising of four circles of radius 9 mm and a rectangle of size 9 mm x 40 mm, was also firmly fixed on the rotatory surface. A plumb statically putted into the sink. A CMOS camera (OS10-V3-4K) with the maximum frame rate 1000 fps was used to collect the images of the plumb line and the rotated mark. Additionally, a DAQ card (INV 3062C) with the maximum sampling rate of 216 kHz collected the output signal of the AUT and the pulse signal of the zero-encoder, and a Polytec interferometer (OFV 5000) was also used to calibrate the AUT for comparison.

Twenty frames of the plumb line were collected when the rotator is stationary, and two hundred frames of the rotated mark were collected at different frame rates for per rotational frequency. The mark images, the output signal of the AUT, and the pulse signal of the zero-encoder for constant four periods were collected at each rotational frequency. The extracted plumb line, the ROI with the four matched circles, and the extracted long edges were shown in Fig. 5. The plumb line slope average value of the twenty frames was taken as the direction of the Earth's gravitational field.

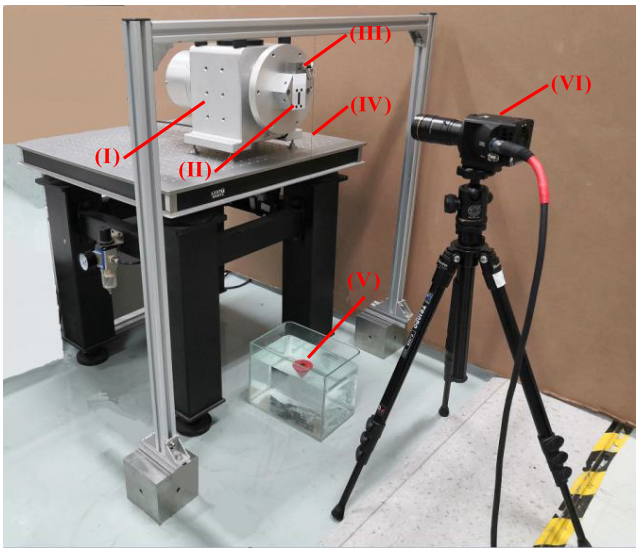

FIGURE 4. Setup for low-frequency accelerometer calibration. (I) Rotator; (II) AUT; (III) mark; (IV) plumb line; (V) sink; and (VI) camera.

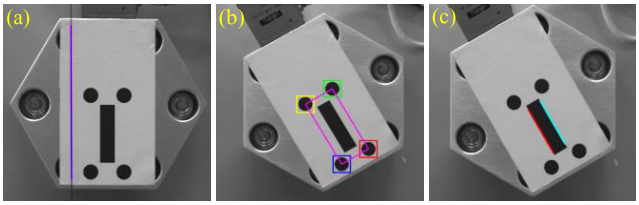

FIGURE 5. The fitted plumb line with the extracted center points by the skeleton extraction method, (b) the matched circles by the template matching and the ROI, and (c) the extracted long edges of the rectangle by the Zernike moment method.

A. SENSITIVITY PHASE AND MAGNITUDE CALIBRATION RESULTS

The sensitivity phase and magnitude of the AUT were calibrated by the MVEG method to validate its calibration accuracy. The rotator applied the sinusoidal acceleration to the AUT in the range from 0.01 Hz to 2 Hz. The MVEG method was used to calibrate the sensitivity phase and magnitude ten times at each frequency at 1/3 octave center frequencies in this range. The calibrated sensitivity phase and magnitude were shown in Fig. 6. The standard deviation (*Std*) of the sensitivity phase at each frequency was less than 0.009°. Compared with the EG described in [14], the MVEG and EG methods have an approximately constant small sensitivity phase difference at each frequency, which caused by the inconsistency between the direction of its reference 0° and that of the Earth's gravitational field. In the entire range, the

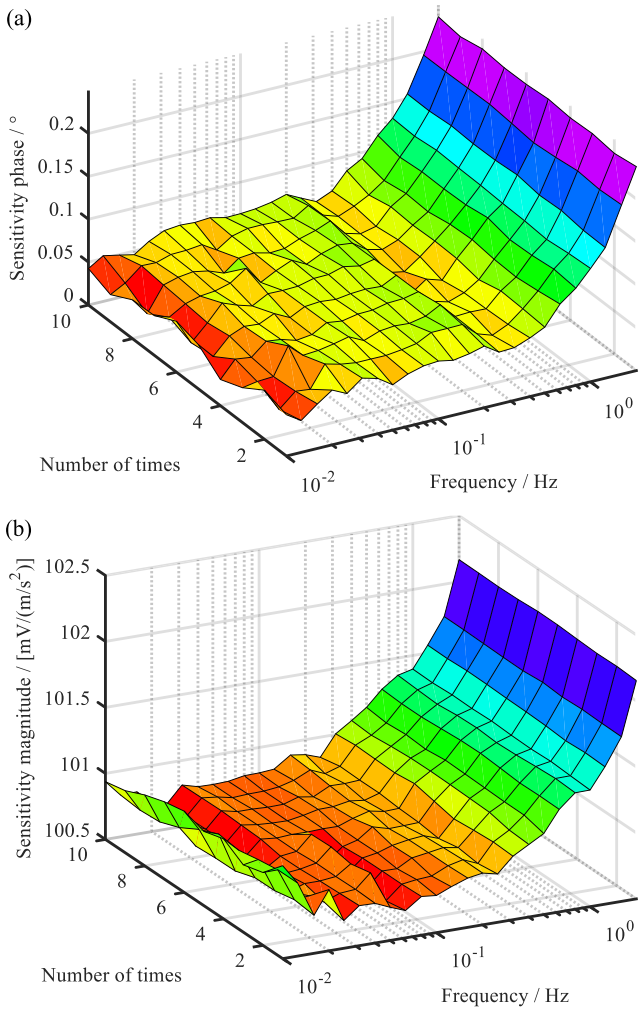

FIGURE 6. Calibrated sensitivity phase and magnitude of the AUT acquired by the MVEG method in the range from 0.01 Hz to 2 Hz. (a) Sensitivity phase, and (b) sensitivity magnitude.

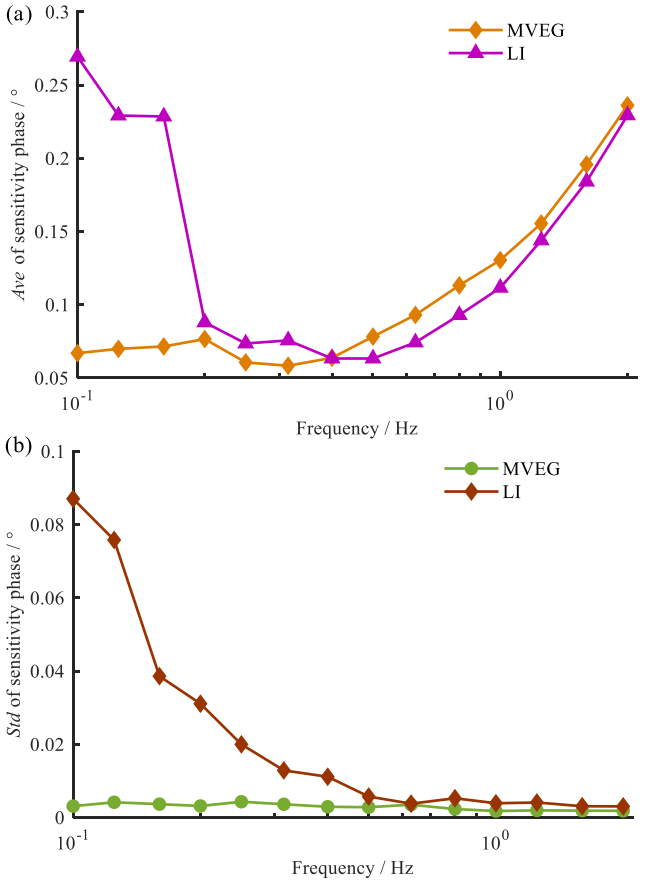

FIGURE 7. Calibrated sensitivity phase of the AUT acquired by the MVEG method and LI in the range from 0.1 Hz to 2 Hz. (a) Ave of the sensitivity phase, and (b) Std of the sensitivity phase.

maximum relative standard deviation (*RStd*) of the sensitivity magnitude was approximately 0.1%.

Because the low SNR of the output signal dramatically affected the calibration accuracy of the LI described in ISO when the frequency is < 0.1 Hz, the sensitivity phase and magnitude of the AUT were calibrated ten times by LI with the range from 0.1 Hz to 2 Hz, instead of the range from 0.01 Hz to 2 Hz. Figures 7 and 8 show the sensitivity phase and magnitude calibrated by the MVEG method and LI, respectively. In the range from 0.1 Hz to 0.3 Hz, the maximum *Std* of the sensitivity phase and maximum *RStd* of the sensitivity magnitude by the MVEG method were 0.004° and 0.021%, which were dramatically less than the corresponding maximum *Std* 0.087° and *RStd* 0.200% of LI. When the frequency is > 0.3 Hz, the *Std* and *RStd* of these two methods were consistent, and the maximum difference of the sensitivity phase average value (*Ave*) and maximum deviation of the sensitivity magnitude *Ave* between the MVEG method and LI were only 0.019° and 0.234%, respectively. It is obvious that the calibration precision in both the sensitivity phase and magnitude by the MVEG method are very similar to that of LI in the range from 0.3 Hz to 2 Hz.

Taking environmental noises, camera distortion, image measurement, AUT output signal measurement, transverse motion, etc as the main uncertainty sources to evaluate the measurement uncertainties of the sensitivity phase and magnitude calibrated by the proposed MVEG method. Meanwhile, the measurement repeatability of the sensitivity phase and magnitude was considered, respectively. Take the uncertainty sources and their corresponding uncertainties of the sensitivity phase as an example, as listed in Table 1. The measurement uncertainty of the sensitivity phase evaluated by the GUM [25] was 0.32°. Similarly, the measurement uncertainty of the sensitivity magnitude was 0.34%.

B. DISCUSSION

Because the SNR of output signal of the AUT is limited by the small excitation acceleration for LI decreases when the frequency is within the range from 0.1 Hz to 0.3 Hz, both *Std* of the sensitivity phase and *RStd* of the sensitivity magnitude by LI are larger than those of the MVEG method, as shown in Figs. 7(b) and 8(b). It is obvious that the calibration accuracy in both the sensitivity phase and magnitude of accelerometer calibration by the MVEG method is higher than that by LI when the frequency is < 0.3 Hz, especially is < 0.1 Hz.

TABLE 1. The uncertainty sources and their corresponding uncertainties.

No.	Symbol	Uncertainty source	Distribution	Uncertainty component (°)
1	$u(en)$	Effect of the environmental noises on the image signal measurement	Rectangle	0.029
2	$u(ec)$	Effect of the camera distortion on the image signal measurement	Rectangle	0.023
3	$u(ev)$	Effect of the vibration on the image signal measurement	Rectangle	0.116
4	$u(ef)$	Effect of the rotational frequency on the image signal measurement	Rectangle	0.012
5	$u(ur)$	Measurement uncertainty of the rectangle long edges in the mark image	Rectangle	0.023
6	$u(eo)$	Other effects on the image signal measurement	Rectangle	0.017
7	$u(er)$	Effect of the rectangle long edges straightness	Rectangle	0.012
8	$u(et)$	Effect of the rotator transverse motion on the image signal measurement	Rectangle	0.017
9	$u(ur)$	Measurement uncertainty of the rotational frequency	Rectangle	0.029
10	$u(fm)$	Effect of the filter on the image signal measurement	Rectangle	0.006
11	$u(us)$	Measurement uncertainty of the output signal of the SUT	Rectangle	0.029
12	$u(em)$	Effect of the rigid modal on the output signal	Rectangle	0.046
13	$u(os)$	Other effects on the output signal	Rectangle	0.058
14	$u(rs)$	Repeatability of the output signal	Normal	0.050
15	$u(rp)$	Repeatability of the sensitivity phase	Normal	0.005
	$u(\varphi_p)$	Combined measurement uncertainty		0.161
	$U(\varphi_p)$	Expanded measurement uncertainty ($k=2$)		0.322

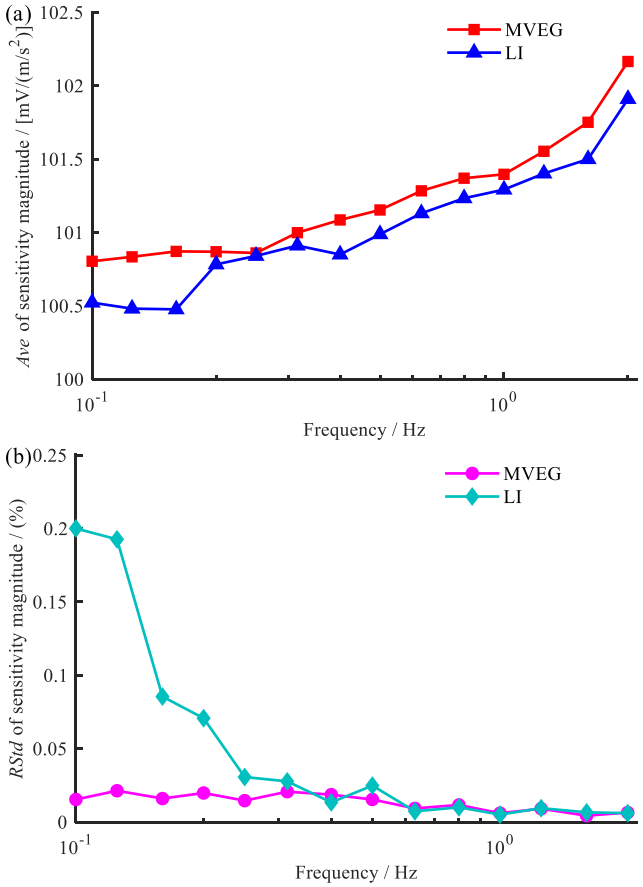

FIGURE 8. Calibrated sensitivity magnitude of the AUT acquired by the MVEG method and LI in the range from 0.1 Hz to 2 Hz. (a) Ave of the sensitivity magnitude, and (b) RStd of the sensitivity magnitude.

The sensitivity phase and magnitude calibrated by the MVEG highly agree well with those by LI in the range from 0.3 Hz to 2 Hz, as shown in Figs. 7 and 8. The *RStd* and *Std* of the MVEG method are very small in the range from 0.01 Hz to 2 Hz, it is suitable for the high-accuracy low-frequency vibration calibration.

V. CONCLUSION

In this study, a monocular vision-based Earth's gravitation method is investigated to accurately calibrate the sensitivity phase and magnitude of low-frequency accelerometer. The MV in this method is used to measure the direction of the Earth's gravitational field and the rotation angle in order to get the accurate excitation acceleration of the AUT. The time-spatial synchronization technique was applied to calibrate the sensitivity phase via the MV measures the aligned spatial position of the excitation acceleration signal with respect to that of the output signal. Experimental results validated that its calibration accuracy in both the sensitivity phase and magnitude of the accelerometer are consistent with that of LI in the range from 0.3 Hz to 2 Hz and the calibration accuracy are especially better than that of LI when the frequency is less than 0.3 Hz.

REFERENCES

[1] W. He, Z. Wang, Y. Mei, and R. Shen, "A novel vibration-level-adjustment strategy for ultralow-frequency vibration calibration based on frequency-shifted method," *Meas. Sci. Technol.*, vol. 24, no. 2, Jan. 2013, Art. no. 025077.
[2] Q. Lu, C. Wang, J. Bai, K. Wang, S. Lou, X. Jiao, D. Han, G. Yang, D. Liu, and Y. Yang, "Minimizing cross-axis sensitivity in grating-based optomechanical accelerometers," *Opt. Express*, vol. 24, no. 8, pp. 9094–9111, Apr. 2016.
[3] A. Sabato, C. Niezrecki, and G. Fortino, "Wireless MEMS-based accelerometer sensor boards for structural vibration monitoring: A review," *IEEE Sensors J.*, vol. 17, no. 2, pp. 226–235, Jan. 2017.
[4] X. Y. Hou, C. G. Koh, K. S. C. Kuang, and W. H. Lee, "Modeling and experimental characterization of a new piezoelectric sensor for low-amplitude vibration measurement," *Meas. Sci. Technol.*, vol. 28, no. 7, Jun. 2017, Art. no. 075106.
[5] T. Bruns, F. Blume, K. Baaske, M. Bieler, and H. Volkers, "Optoelectronic phase delay measurement for a modified michelson interferometer," *Measurement*, vol. 46, no. 5, pp. 1762–1765, Jun. 2013.

[6] N. Garg and M. I. Schiefer, "Low frequency accelerometer calibration using an optical encoder sensor," *Measurement*, vol. 111, pp. 226–233, Dec. 2017.

[7] *Methods for the Calibration of Vibration and Shock Sensors—Part 11: Primary Vibration Calibration by Laser Interferometry*, Standard ISO 16063-11, International Standardization Organization, 1999.

[8] *Methods for the Calibration of Vibration and Shock Transducers: Part 41. Calibration of Laser Vibrometers*, Standard ISO 16063-41, International Standardization Organization, 2011.

[9] Y.-B. Lee, H. C. Kim, and S.-W. Kim, "Determination of the sensitivity phase of an accelerometer based on an analysis of the harmonic components of the interference signal," *Meas. Sci. Technol.*, vol. 19, no. 4, Feb. 2008, Art. no. 045204.

[10] D. A. Scott and L. P. Dickinson, "Distortion effects in primary calibration of low-frequency accelerometers," *Metrologia*, vol. 51, no. 3, pp. 212–224, May 2014.

[11] N. Garg, O. Sharma, A. Kumar, and M. I. Schiefer, "A novel approach for realization of primary vibration calibration standard by homodyne laser interferometer in frequency range of 0.1Hz to 20 kHz," *Measurement*, vol. 45, no. 8, pp. 1941–1950, Oct. 2012.

[12] M. Yang, Y. Wang, C. Cai, Z. Liu, H. Zhu, and S. Zhou, "Monocular vision-based low-frequency vibration calibration method with correction of the guideway bending in a long-stroke shaker," *Opt. Express*, vol. 27, no. 11, pp. 15968–15981, May 2019.

[13] T. Bruns and S. Gazioch, "Correction of shaker flatness deviations in very low frequency primary accelerometer calibration," *Metrologia*, vol. 53, no. 3, pp. 986–990, Jun. 2016.

[14] J. Dosch, "Low frequency accelerometer calibration using earth's gravity," in *Proc. 25th Conf. Expo. Struct. Dyn. (IMAC)*, 2007, pp. 1–6.

[15] M. Lu, S. Wang, L. Aulbach, M. Jakobi, and A. W. Kochs, "Non-phase unwrapping interferometric approach for a real-time in-plane rotation measurement," *Opt. Lett.*, vol. 42, no. 10, pp. 1986–1989, May 2017.

[16] H. Dong, Q. Fu, X. Zhao, Q. Quan, and R. Zhang, "Practical rotation angle measurement method by monocular vision," *Appl. Opt.*, vol. 54, no. 3, pp. 425–435, Jan. 2015.

[17] H. Kim, Y. Yamakawa, T. Senoo, and M. Ishikawa, "Visual encoder: Robust and precise measurement method of rotation angle via high-speed RGB vision," *Opt. Express.*, vol. 24, no. 12, Jun. 2016, Art. no. 263175.

[18] G. Hussain and M. Ikram, "Optical measurements of angle and axis of rotation," *Opt. Lett.*, vol. 33, no. 18, pp. 2419–2421, Sep. 2008.

[19] W. Li, J. Jin, X. Li, and B. Li, "Method of rotation angle measurement in machine vision based on calibration pattern with spot array," *Appl. Opt.*, vol. 49, no. 6, pp. 1001–1006, Feb. 2010.

[20] J. Jin, L. Zhao, and S. Xu, "High-precision rotation angle measurement method based on monocular vision," *J. Opt. Soc. Amer. A, Opt. Image Sci.*, vol. 31, no. 7, pp. 1401–1407, Jul. 2014.

[21] S. Korman, D. Reichman, G. Tsur, and S. Avidan, "Fast-match: Fast affine template matching," *Int. J. Comput. Vis.*, vol. 121, no. 1, pp. 111–125, Jan. 2017.

[22] G. A. Papakostas, Y. S. Boutalis, D. A. Karras, and B. G. Mertzios, "A new class of Zernike moments for computer vision applications," *Inf. Sci.*, vol. 177, no. 13, pp. 2802–2819, Jul. 2007.

[23] A. Bera, P. Klesk, and D. Sychel, "Constant-time calculation of Zernike moments for detection with rotational invariance," *IEEE Trans. Pattern Anal. Mach. Intell.*, vol. 41, no. 3, pp. 537–550, Mar. 2019.

[24] M. Yang, H. Zhu, C. Cai, Y. Wang, and Z. Liu, "Bandpass-sampling-based heterodyne interferometer signal acquisition for vibration measurements in primary vibration calibration," *Appl. Opt.*, vol. 57, no. 29, pp. 8586–8592, Oct. 2018.

[25] *Evaluation of Measurement Data—Guide to the Expression of Uncertainty in Measurement*, document JCGM 100, 2008.

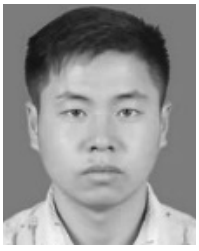

MING YANG received the B.E. degree from the College of Information Science and Technology, Beijing University of Chemical Technology, Beijing, China, in 2014, and the M.S. degree from the Control Science and Engineering Department, Beijing University of Chemical Technology, in 2016, where he is currently pursuing the Ph.D. degree with the Control Science and Engineering Department. His main research interests include machine vision and vibration metrology.

HAIJIANG ZHU received the Ph.D. degree in pattern recognition and intelligent system from the National Laboratory of Pattern Recognition, Institute of Automation, Chinese Academy of Sciences, Beijing, China, in 2004. From 2006 to 2007, he was a Visiting Scholar with the Faculty of Engineering, Iwate University, Japan. He is currently a Professor at the College of Information Science and Technology, Beijing University of Chemical Technology. His research interests include image processing and computer vision.

CHENGUANG CAI received the Ph.D. degree in precision instrumentation and mechanics from the School of Instruments Science and Optoelectronic Engineering, Beihang University, Beijing, China, in 2007. From 2007 to 2009, he worked at Nokia Research Center, Beijing, where he held a postdoctoral position. He is currently an Associate Research Fellow at the National Institute of Metrology, China. In 2016, he was a Visiting Scientist at the Physikalisch-Technische Bundesanstalt, Germany. His research interest includes vibration calibration.

YING WANG received the Ph.D. degree in precision instrumentation and mechanics from School of Instruments Science and Optoelectronic Engineering, Beihang University, Beijing, China, in 2006. From 2015 to 2016, she was a Visiting Scholar with Johns Hopkins University, USA. She is currently an Associate Professor at the Institute of Microelectronics, Chinese Academy of Sciences, Beijing. Her research interests include machine vision and image processing.

ZHIHUA LIU received the B.E. degree from Jilin University, Jilin, China, in 2010, and the Ph.D. degree from Tsinghua University, Beijing, China, in 2015. From 2015 to 2017, he was a Postdoctoral Research Fellow with the National Institute of Metrology, Beijing, where he is currently an Associate Research Fellow. His research interests include sensor testing theory and method, and the development of testing equipment design and control.

SHENGYANG ZHOU received the B.E. degree from the College of Information Science and Technology, Beijing University of Chemical Technology, Beijing, China, in 2016, and the M.S. degree with the Control Science and Engineering Department, Beijing University of Chemical Technology, in 2019. His research interests include sensor testing theory and method, and the development of testing equipment design and control.